The Computation of Ocean Wave Heights From GEOS-3 Satellite Radar Altimeter Data

J. F. R. GOWER

Institute of Ocean Sciences, Patricia Bay, P.O. Box 6000, 9860 W. Saanich Road, Sidney, British Columbia V8L 4B2, Canada

The GEOS-3 satellite, carrying a short pulse radar altimeter, was launched into orbit round the earth in April 1975. The altimeter was designed to provide an accurate measurement of the distance of the satellite above the earth, and also to record the shape of the radar return pulse as a measure of the mean roughness of the earth's surface. The satellite is intended to operate over the oceans, where surface height changes show variations in the earth's gravitational field, and roughness changes are due to waves.

This paper is concerned with methods of determining waveheights from the shape of the radar return pulse and the corrections that have to be taken into account. The effects of timing variations on the shape of the average return pulse shape are discussed in detail. Accurate calibration of the sampling gates that measure this shape is found to be particularly critical.

The waveheights deduced are compared with ground truth derived from ship reports on waveheights in the N.E. Pacific Ocean and routine measurements made at Ocean Weather Station PAPA. It is found that with suitable calibration and adjustments, the satellite measurements agree with surface observations to about 0.5 meters in $H_{\frac{1}{3}}$.

Introduction

Greenwood et al. in two papers (1969a and b) reviewed the uses of sea surface height information that might be obtained by satellite altimetry. This height shows the shape of the geoid combined with the effects of wind, tides, and currents. In addition, the shape of the reflected pulse can be used to indicate mean surface roughness, which over the sea is a measure of waveheight. Various studies of the measurement of pulse shape were made in the early stages of the GEOS-3 project (Shapiro, Uliana and Yaplee 1972; Miller and Mayne, 1972; Barrick, 1972). The basic analysis uses linear scattering theory and effectively assumes that the incident microwave energy is, on average, reflected back to the satellite equally for all elements of the sea surface. Within a small area directly beneath the satellite the distribution of instantaneous sea surface heights due to waves causes a distribution of ranges for the reflected energy. Reflections with longer time delays also occur from the roughened surface at angles further off nadir.

With the assumption of uniform reflectivity the actual shape of the return pulse is proportional to the area of sea surface illuminated at any given time. For a narrow transmitted pulse and a calm but slightly roughened sea, this shape will approximate a step function, since the area of ocean illuminated is initially a dot and then a spreading ring whose area remains constant. With increasing waveheight the rise time of the step is lengthened, and for a gaussian transmitted pulse shape and gaussian sea surface height distribution, the return pulse approximates a modified error

 0034-4257/79/020097+18$01.75

function of the form (Brown 1977):

$$S(t) = S_0 + \frac{S_1}{2\pi} \int_{-\infty}^{t} e^{\frac{-(t'-t_0)^2}{2\sigma^2}} dt' \quad (1)$$

where

S_0 is the signal level before pulse arrival due to receiver noise and offset;
S_1 is the signal increase when the pulse is received; this increase is from S_0 to the plateau value $S_0 + S_1$;
t_0 is the mean arrival time, when the average signal has increased from S_0 by $S_1/2$;
σ is the standard deviation of the leading edge shape to which waveheight and transmitted pulse length contribute; and
t and t' are time variables.

For the waveheight analysis only the value of σ is required, and this would be found by a fitting process or maximum likelihood estimation from the observed pulse shape.

GEOS-3 radar altimeter data are collected in a variety of modes. For obtaining waveheight information the altimeter must operate in the 'intensive' mode where the transmitted pulse width is nominally 12.5 nsec ($\sigma_p = 5.4$ nsec) rather than in the lower power 'global' mode where a 200 nsec pulse is used. Data from this intensive mode operation can then be telemetered to earth at either the 'low' or the 'high' data rates. In the low data rate mode only average pulse shape information, as computed on the satellite, is available at 2-sec intervals. In the high data rate mode the same averages are given at 3.2-sec intervals, and in addition the shapes, timing errors, and other information are given for the individual pulses. One hundred pulses are recorded

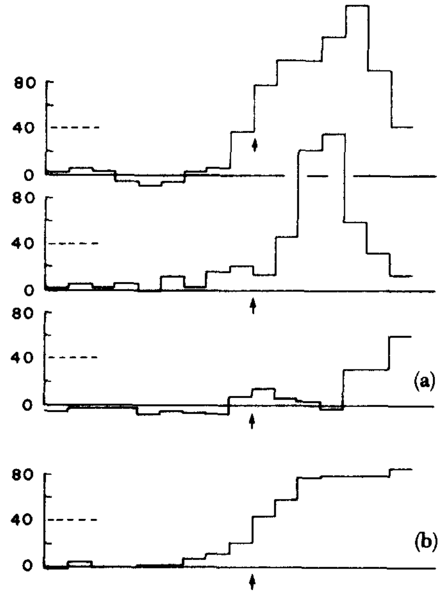

FIGURE 1. (a) Typical leading edge shapes of individual pulses plotted from the 16 samples of received signal power. (b) An average of 320 pulses similar to those shown in (a) plotted with the same vertical scale. The small vertical arrows indicate the sample number corresponding to the parameter t_0 in Eq. 1.

per second in segments of 3.2 sec (320 pulses).

Returns from these individual pulses are extremely variable. The post detection bandwidth is almost as large as the intermediate frequency bandwidth, so that samples of the final signal will have standard deviations comparable to their mean values. Typical observed pulse shapes are shown in Fig. 1(a). This shape is sampled by 16 gates spaced at 6.25-nsec intervals with the midpoint of the rise of the leading edge (t_0) arranged to occur near sample gate number 10. Time variables are often expressed in units of the sample interval.

Calculations on the data show that the standard deviations of the signal recorded by the later sampling gates for a single pulse are equal to about 60% of the mean value, and many pulses have to be averaged before waveheights can be computed with any accuracy. The mean shape of 320 pulses is shown in Fig. 1(b). This can be fitted by the error function given in Eq. 1 with approximate values $S_0 = 2$ units, $S_1 = 80$ units, $t_0 = 10$ sample intervals, $\sigma = 1.4$ sample intervals (8.75 nsec).

The average pulse shape will be subject to an additional increase in the apparent value of σ due to any uncorrected timing variations between pulses. The average pulse shapes given on the GEOS-3 data tapes are not corrected for these relative timing errors. The complete 'high' data rate format includes enough data to recalculate a corrected average as described below, but with the 'low' data rate format in which most data are available, no such correction is possible.

Timing of the sampling gates relative to the leading edge of the return pulse is accomplished by a tracking loop that adjusts the delay between the time of transmission and the time of sampling by the gates so that the midpoint of the steeply rising leading edge of the pulse is received near the center of the sampled time interval. Timing is adjusted by range servo error signals calculated from the ratio of the signal in a gate on the rising edge of the pulse to the signal in a gate 62.5 nsec later when the return pulse will have reached its plateau value. The bandwidth of the tracking loop is about 4 Hz, large enough to follow variations due to range changes over the ocean and, in some cases, over the land. The use of such a split gate tracker has been studied by Hofmeister (1976). Godby (1976) presented data on standard deviation of the loop jitter (σ_j) measured on the GEOS-3 altimeter before launch as a function of the σ value (Eq. 1) of the leading edge being tracked. He showed that σ_j will vary with waveheight, since as the waveheight increases, the leading edge of the pulse becomes less sharp and timing jitter tends to increase. The data given by Godby are plotted as the dashed curve in Fig. 10 and are discussed below.

The measured value of σ will now be a combination of the standard deviations of transmitted pulse shape (σ_p), the range of delays caused by the sea surface wave height distribution (σ_s), and the timing loop jitter (σ_j). The transmitted pulse shape for the intensive mode has been measured to have an accurately gaussian shape. The sea surface height distribution has been found to be gaussian with the magnitude of skew and kurtosis parameters less than 0.2. This results in a maximum deviation from a gaussian shape of 2.5% of the peak value which is too small to be seen on the GEOS-3 data, σ_j results from a random electronic process and represents a gaussian distribution of timing errors. Convolution of the transmitted gaussian pulse by the two gaussian time distributions results in:

$$\sigma^2 = \sigma_p^2 + \sigma_s^2 + \sigma_j^2$$

The usual classification of waveheights that correspond easily to visual observations of the random wave surface as measured against a vertical fixed scale is by the mean height of the largest 1/3 of the waves. This parameter ($H_{\frac{1}{3}}$) can be computed for a measured wave sequence and has been found to equal 4 σ_s where σ_s is now a length measurement (Longuet-Higgins, 1952; Wilson and Baird, 1972). The conversion between time and distance for a radar altimeter is by one-half the velocity of light (allowing for two-way travel time for the radar). One nanosecond therefore represents a 0.15 m range difference so that $H_{\frac{1}{3}}$ (meters) = 0.6 σ_s (nanoseconds). Hence

$$H_{\frac{1}{3}} = 0.6\sqrt{\sigma^2 - \sigma_p^2 - \sigma_i^2} \text{ meters} \quad (2)$$

for $\sigma, \sigma_p, \sigma_i$ in nanoseconds.

GEOS-3 Wave Data

Figure 2 shows the area of the NE Pacific considered in this study and the orbital tracks of GEOS-3 with their times (GMT) on a typical day (April 30, 1975). Three descending orbits (dashed) 1 hour 40 minutes apart are followed by two ascending orbits (solid lines) about 6 hours later. Waveheight measurements are made only along the satellite track.

The diameter of the 'footprint' of the radar altimeter depends on what range of time delays are important in the waveheight calculations. This range, taken to be $2 \times \sigma_s$ with $H_{\frac{1}{3}} = 5$ m, gives a footprint diameter of about 5 km. For a calm sea this value would be about 2 km. These values are narrower than the lines in the figure. Along the track, pulses are transmitted 100 times per second or at intervals of roughly 1/10 km so that footprints overlap greatly. The standard data segment length 3.2 sec used in the NASA data format, produces values of waveheight averaged over distances of about 25 km, which should be sufficiently frequent to follow most waveheight variations caused by surface winds. Large areas remain uncovered between the tracks if data are available from a single satellite only. An operational system such as is planned for SEASAT, however, would include 3 satellites and the capability for extrapolating measurements to either side of the track using other sensors.

Figure 3 is a typical wave chart for

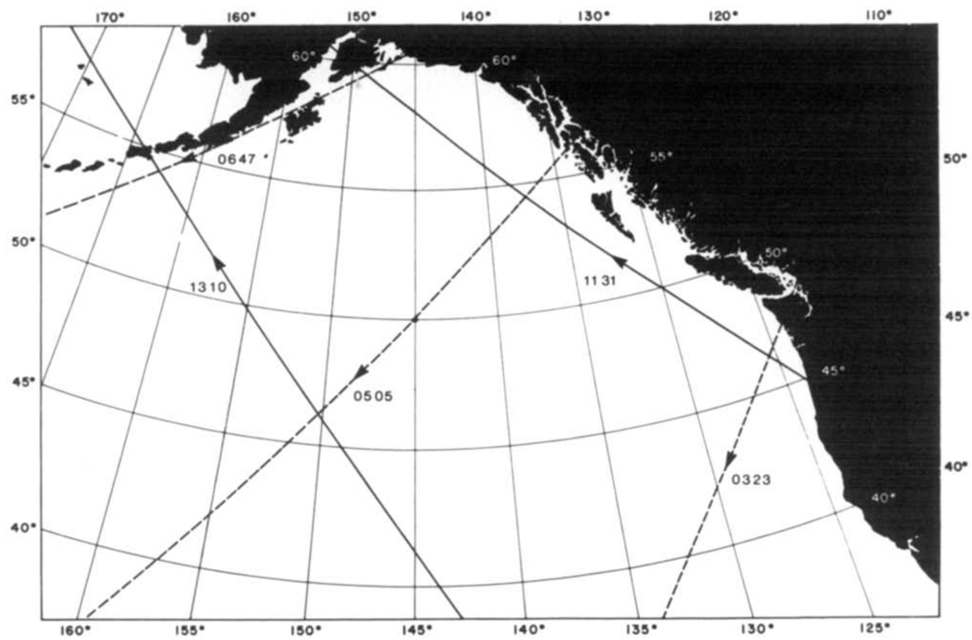

FIGURE 2. The area of the NE Pacific studied with typical GEOS-3 orbit tracks. Ascending orbits (solid lines) and descending orbits (dashed) are shown with their approximate times GMT on 30 April 1975.

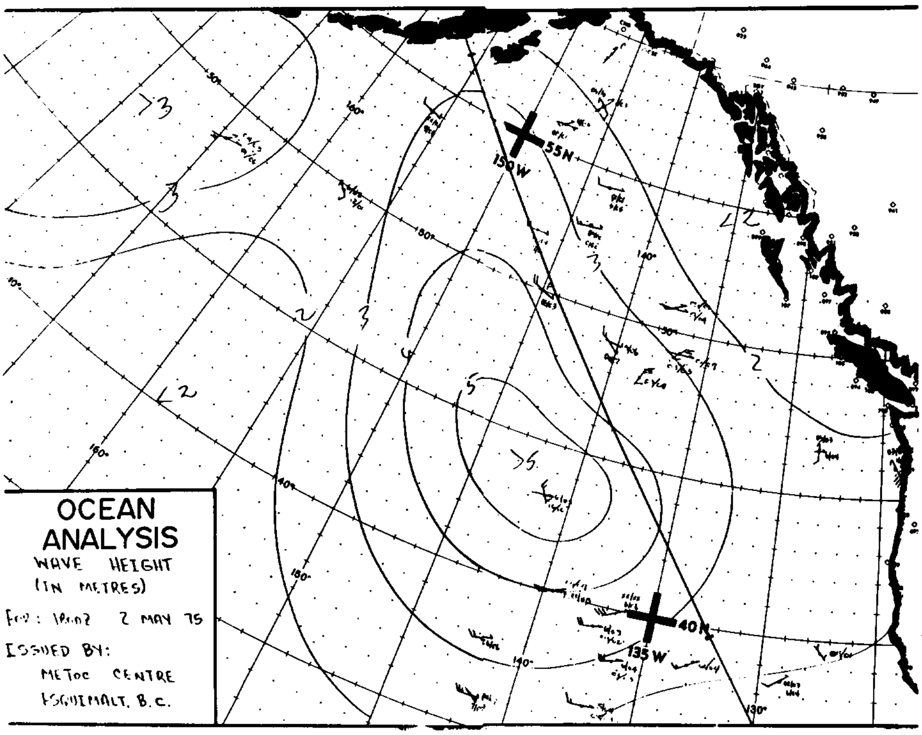

FIGURE 3. The waveheight chart produced by the Canadian Forces Metoc Centre for this area at 1800 hr GMT on May 2, 1975, showing the GEOS-3 orbital track followed at about 1232 GMT on that day.

the area, produced twice daily by the Canadian Forces Meteorology and Oceanography Centre in Esquimalt, B.C. Contours are the waveheights ($H_{\frac{1}{3}}$) in meters compiled from ship reports at 1800 GMT on May 2, 1975. Locations of the reporting ships are shown by the wind and wave flags which indicate the reported data. Wind speed and direction, and the significant height, direction, and period of 'sea' waves and swell are all reported. Most wave data are visual estimates made by officers from the ship's bridge. The waveheight ($H_{\frac{1}{3}}$) data plotted for station PAPA, however, are read from an analog display of the on-board N.I.O. Tucker wavemeter. The total waveheights contoured are a combination of sea and swell.

It can be seen that the waveheight contours are drawn from a very sparse scattering of ship reports. Wind predictions using barometric pressure reports and satellite images of atmospheric fronts and pressure system locations are also used in compiling the wave charts, but the accuracy of the ground truth at different points along the satellite track is clearly very variable.

The GEOS-3 satellite passed over the track shown on Fig. 3 at 12.32 GMT on the same day, May 2, 1975. Data for the pass were received at NASA Goddard and processed at NASA Wallops before distribution on industry compatible magnetic tapes. The processing involves applying calibration corrections to the data, adding predicted orbit information, and computing a waveheight based on the calculations described in the previous section. This computed waveheight appears on the data tapes and is shown

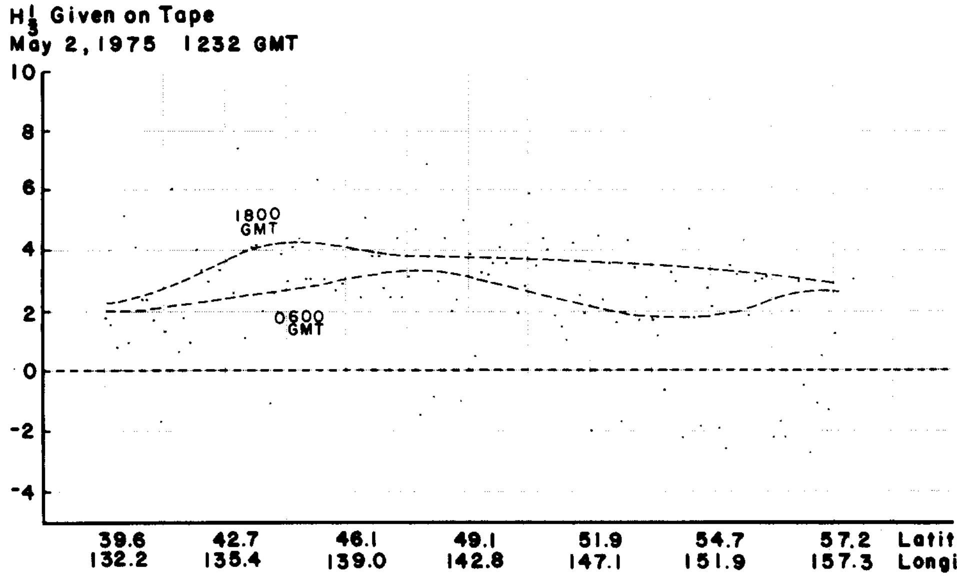

FIGURE 4. The values of $H_{\frac{1}{3}}$ in meters given on the NASA data tape for the pass whose track is plotted in Fig. 2. Waveheights read from Fig. 2 and from a similar chart compiled for 0600 hr are shown as dashed lines.

plotted against satellite position in Fig. 4. The dashed lines are derived from the waveheight contours in Fig. 3 and from an earlier chart compiled from observations at 0600 GMT the same day. The track passes near Station PAPA (50°N, 145°W) where observations show that at 1200 GMT the waveheight was intermediate between these two lines.

The scatter of these satellite measurement points is large, which greatly reduces the usefulness of the data. The algorithms used for computing waveheight must therefore be critically examined for points where improvements can be made.

One method of deriving waveheights uses a gaussian fitting technique (Barrick, 1972) and is illustrated in Fig. 5. Here the shapes of individual pulses as defined by 16 samples of the leading edge have been averaged and the resulting mean pulse differentiated by computing the difference between successive sample values to produce the 'noisy' gaussian shape shown. A standard least-squares program is then used to fit a gaussian curve to this shape with the resulting height, position, and standard deviation indicated. Errors in these quantities are also given. The times for position and standard deviation are given in units of the sample interval of 6.25 nsec. Since differentiation of the error function in Eq. 1 produces a gaussian function with the same σ and t_0 values, the gaussian fit technique provides a simple method of estimating these quantities.

Waveheights are calculated from the σ value using Eq. 2. For the values given on the data tapes no correction was made by NASA for timing jitter (i.e. $\sigma_j =$ 0 is assumed) and σ_p was taken to be 8.55 nsec. Since the nominal shape of the transmitted pulse has $\sigma_p = 5.4$ nsec, the larger value used would allow for a fixed additional amount of broadening due to timing variations and other causes.

When this gaussian fit technique is used to derive waveheights from the ana-

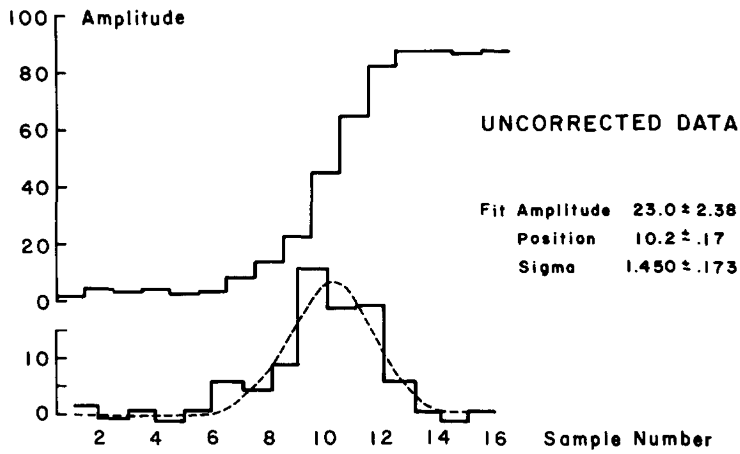

FIGURE 5. The average leading edge shape of 320 pulses (3.2 sec of data) is averaged to form the top trace. A gaussian curve (dashed) is fitted to the differential of this trace shown just below it. Parameters and errors of the best-fitting curve are shown to the right.

log average pulse shapes given on the tape, the σ values produced give waveheights with similar scatter to those shown in Fig. 4, that is, 1.6 m about a 5 number running mean. Improved processing methods that reduce this scatter are discussed below, and the reductions achieved with each step are given.

Some scatter is inherent in the fact that the random sea surface height distribution is being measured. In conventional wave recording, a time series of surface elevations is usually taken for 15 to 20 min in order to reduce expected random fluctuations in the measurement of H 1/3 to below 10%. In a satellite altimeter the averaging is over an area of ocean rather than a period of time. The effective footprint of the GEOS-3 altimeter has a diameter in the range 2–5 km, increasing for larger waves. An average over 2 sec in moderate wave conditions means that about 60 km^2 of area are being sampled by the altimeter. Rough calculation shows that this implies about 10 times the averaging obtained in 15 min of observations at one location. Fluctuations due to other electronic effects discussed below are therefore expected to dominate.

The mean values of derived waveheights depend on the values taken for σ_p and σ_j in Eq. 2. Laboratory measurements with the altimeter in 'calibration' mode confirmed the nominal $\sigma_p = 5.4$ nsec, but the manufacturers have stated that this value will be slightly larger in actual operation. The present study shows that $\sigma_p = 6.35 \pm 0.25$ nsec gives the best fit to ground truth. Prelaunch measurements of timing jitter showed σ_j to have values plotted as the dashed line in Fig. 10. This study confirms these values, but shows that the timing variations they represent can in fact be corrected in detail.

Improved Algorithms for Computing Waveheight

If only the 'low rate' data are available then no better estimates of pulse broadening effects due to timing variations can be made. Various improvements in the fitting procedure for deducing the value of σ from the given pulse shapes can however be tested.

The first possible improvement is to try to fit the form of Eq. 1 directly to the pulse shape. The gaussian fit method described above has the advantage that offsets in signal level (S_0) of the average shape are automatically removed, and that a gaussian fit routine is easy to implement. Fitting the 16 sample values to a modified error function before differentiation would, however, be more direct and would avoid the approximations involved in the very coarse differentiation used. The error function is not analytic, but suitable digital approximations are given in Abramovitz and Stegun (1964). Some large computers also have the error function directly available in the FORTRAN compiler. Differential coefficients of the error function required by some fitting programs are analytic. The base-line level (S_0) needs to be introduced as a fourth parameter in fitting the error function since this level is found to vary in the data.

Tests with the two methods of fitting using modeled pulse averages with added noise show that the error function provides a fit with about 0.8 of the error resulting from fitting a gaussian to the differentiated shape. The gaussian fit also overestimates the standard deviation slightly. This effect would be important at low waveheights, where it is equivalent to 1 meter of waveheight over a calm sea, but decreases to less than 5% for true waveheights greater than 3 m.

A further improvement should result from weighting the sample values by the reciprocal of the observed variance in the data from each gate. The weighting particularly emphasizes data from samples at the start of the leading edge where signal levels and the associated standard deviations are both low. This is proposed in the "GEOS-C Data users handbook" (Hofmeister et al., 1976) and tests on ideal model data confirm that an improvement corresponding to a reduction in errors by a factor 0.6 does occur. In practice, however, the problem is complicated by bias errors in the data from individual gates, which effectively increase the signal variations in all gates to a higher and more uniform set of values. Detailed correction of these errors is therefore needed.

Notice of bias and timing errors in the individual sampling gates was circulated by NASA in December 1976. The timing errors that had been discovered are plotted in Fig. 6a. The first two gates are

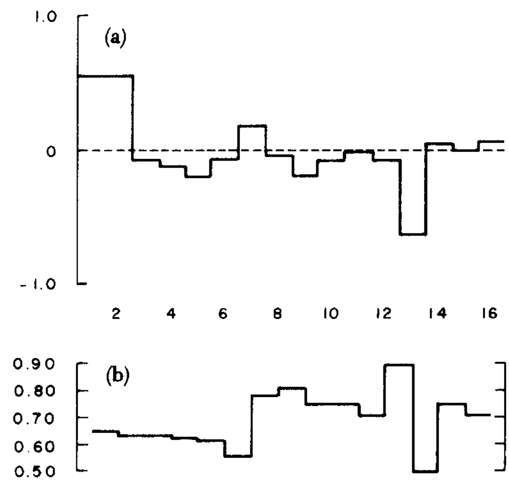

FIGURE 6. (a) Timing errors in the gates used to sample the GEOS-3 return pulse shape. Errors are plotted as fractions of the time interval between gates (6.25 nsec) for each of the 16 gates. The timing of gate 13 is too early by about 4 nsec. (b) The correlation coefficients between adjacent pairs of gates computed from 23000 consecutive return pulses. Data from gate 13 are seen to correlate more strongly with data from gate 14 because of the timing error shown in (a). The mean correlation level of 0.7 is a function of receiver bandwidths.

misplaced relative to the rest by over half a sample interval, but data from these two are not critical for waveheight calculations. Gate 13 is positioned about 2/3 of a sample separation too early. Since this gate is near the center of the sampled interval, errors in its position are much more critical.

The existence of these timing errors can be confirmed in the 'high rate' data by computing correlation coefficients between individual pulse shape data from adjacent gates, as shown in Fig. 6b. Here the effect of the timing error of gate 13 shows clearly. Data from this gate correlate better with data from gate 12 than with that from gate 14. The effects of errors in gates 7 and 9 can also be seen, but the large timing errors in gates 1 and 2 give no effect. The signal in these gates is low and is determined almost entirely by receiver noise, and the correlation coefficients will be strongly affected by the signal digitization.

Recommended bias level corrections were also given by NASA, and are plotted in Fig. 7b. Here Fig. 7a shows an average pulse leading edge shape computed from the data used in Fig. 6. When the bias level corrections plotted below (Fig. 7b) are subtracted, the distortions in the average shape due to consistent small offsets in the data from different gates are reduced by about a factor 2. It can be seen, however, that some steps between signal levels in early and late gates, will remain.

It is difficult to investigate the effects of both timing and bias errors together, and it appears that the timing errors are in any case now reasonably well determined. Assuming the timing error estimates to be correct, it is possible to look for further processing improvements by trying other sets of bias corrections.

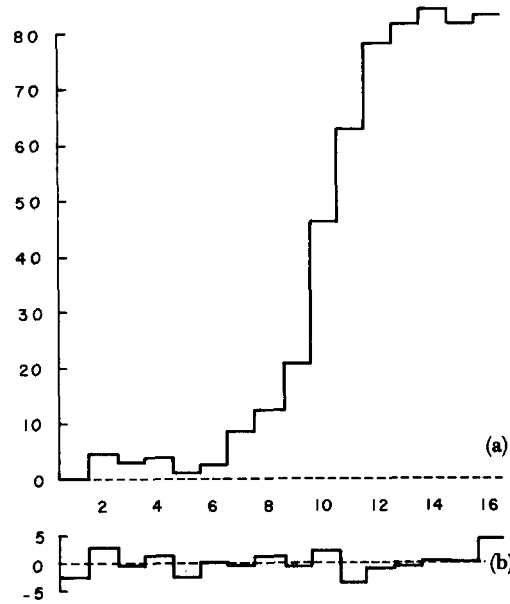

FIGURE 7. (a) The average return pulse shape derived from data used in Fig. 6. The vertical scale is in millivolts of receiver output. The noise level for such a long average should be very low, less than 0.1 units for the early gates and 0.5 units for the later gates. The residual steps are due to consistent offsets in the data from the different gates. (b) Proposed values given by NASA for these offsets. Subtraction of the levels plotted in (b) from those in (a) will reduce the residual steps in the early and late gates by about a factor 2.

Such corrections can be calculated so as to adjust a single average pulse shape to fit an assumed waveheight exactly. If σ, S_1, S_0, and t_0 in Eq. 1 are known and constant for a given section of satellite data, then the expected form of the average pulse shape can be computed incorporating the above timing errors. Deviations between this shape and that observed may then be ascribed to bias errors in each of the 16 sampling gates and improved corrections can be deduced. A section of data was selected from a pass on May 5, 1975, when ship and station PAPA reports indicated a relatively constant waveheight of 2.2 m. If σ_p is taken as 6.35 nsec and the timing

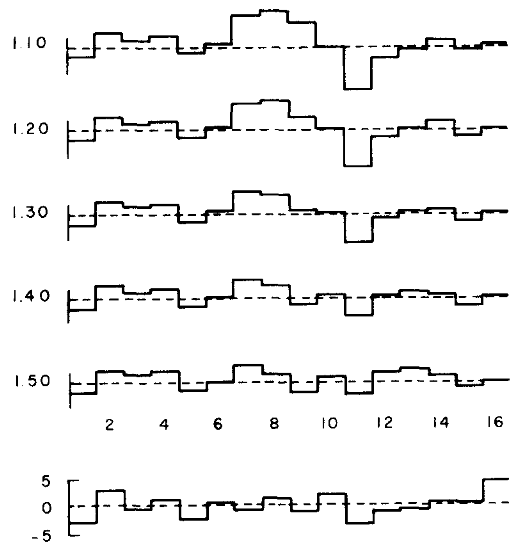

FIGURE 8. Bias level corrections computed so as to give mean pulse shapes with σ values equal to 1.10, 1.20, 1.30, 1.40, and 1.50 for the average shape shown in Fig. 7. The corrections plotted in Fig. 7b are replotted below to the same scale for comparison.

jitter, σ_j, as 4.0 nsec then σ should be 8.35 nsec or 1.336 sample intervals. Figure 8 shows bias values derived to give σ values of between 1.1 and 1.5 sample intervals for this data. It can be seen that the sets of bias values are very similar even though the resulting waveheights ($H_{\frac{1}{3}}$) would be calculated as -1.2 to $+3.4$ m for this range of σ values. This variation in calculated waveheight could be largely compensated by different choices of σ_p, and variations in sample gate bias levels may be contributing to the increase in σ_p above the nominal value that is found in this study.

Bias corrections appropriate to $\sigma=$ 1.336 sample intervals were derived from the May 5 data and tested by applying them to data obtained on May 2. This was found to reduce the residuals remaining after fitting the function in Eq. 1, by about a factor 5, but did not result in a similar improvement in the estimation of σ. Neither the estimated error in this quantity nor its observed variability about a smooth curve showed any noticeable reduction. Both the correction set recommended by NASA and that derived here gave the same factor 0.8 reduction in scatter when used with the weighted fitting algorithm described above.

Although the above discussion has made use of individual pulse shape data that are only available in the "high rate" data format, the object has been to improve processing of "low rate" data in which only average pulse shapes are available. The best technique found in this study for processing this data involves correction of bias and timing errors using either recommended or derived values, followed by a weighted fit to the modified error function of Eq. 1. Errors in sample gate timing can be allowed for very simply if this function is fitted directly, in contrast to the differentiation and gaussian fitting method described initially.

Waveheights computed in the above way were found to show a scatter about a 5 number running mean of roughly 1.2 meters rms compared to the 1.6 meters appropriate to the data in Fig. 4.

Use of "High Rate" Data to Improve Waveheight Estimates

In those cases where satellite data are available in the "high rate" format, further improvements in waveheight estimations can be achieved. In this format 16 data samples are given for the leading edge shape of every pulse return which occurs at the pulse repetition frequency of 100 per second. The 'low rate' data discussed above give only the average pulse shapes which are produced by analog averaging on board the satellite. Since the averages are transmitted to the ground every 2.0 seconds, the low rate data are much more compact and therefore easy to process.

The analog averages are produced on the satellite with a time constant of about 1 sec so that roughly half of the information is being lost when these are only transmitted every 2.0 sec. In the high rate mode the averages are transmitted only every 3.2 sec. The loss of data can now be demonstrated by calculating digital averages of the 320 pulse shapes given in the high rate format for each 3.2-sec segment of data, and comparing the derived waveheights with those computed at NASA from analog averages of the same data. The scatter in the recomputed waveheight about a 5 point running mean is found to be reduced by about a factor 1.5, roughly consistent with the factor $\sqrt{3.2}$ which might be expected from averaging random variations in 3.2 times the amount of data.

A further improvement in data processing which can be made with the high rate data is to make a detailed correction for the effect of timing jitter on the average pulse shape. When the sets of 16 numbers representing the individual pulse shapes are examined it is evident that time excursions of one to two sample intervals occur in the timing of the leading edge on a time scale of about 0.1 sec. This would suggest a value of σ_j on the order of 3 to 5 nsec. A digital algorithm was devised for tracking these timing changes as they appear on the individual return pulse shape data. This algorithm used a combination of incoherent averaging, timing of threshold crossing and subsequent smoothing of the crossing times. The choice of the parameters of the algorithm, the length of the incoherent average, the threshold amplitude, and the smoothing time, were based on the results of tests on model GEOS-3 data.

The algorithm used a relatively low threshold for tracking the leading edge to take advantage of the fact that the signal level is very low before the leading edge arrives, but becomes very variable afterwards. This and the fact that the analysis is not restricted to real time operation give the algorithm two advantages over the split gate tracker that is used on board the spacecraft.

Once the timing variations have been calculated, they can be taken into account in recomputing the average pulse shape. This recomputed pulse shape is found to be narrower and smoother than the original average.

Figure 9 demonstrates the improvement this recalculation makes over the simple digital average of Fig. 5. The differential of the leading edge shape is still subject to coarse quantization by the relatively small number of sample gates, but it is now fitted by a taller, narrower gaussian shape with considerably smaller errors in all 3 parameters. The most important improvement is a factor 2.5 reduction in the predicted error in σ.

The mean reduction in this predicted error for the whole of the satellite pass is by a factor of about 0.6. The standard deviation of the timing variations found for the example in Fig. 9 was 4.4 nsec, in agreement with the predicted value given by the dashed line in Fig. 10. The scattered points in this figure correspond to values of this standard deviation found for each data segment in the pass. The points in general fall within about 1.5

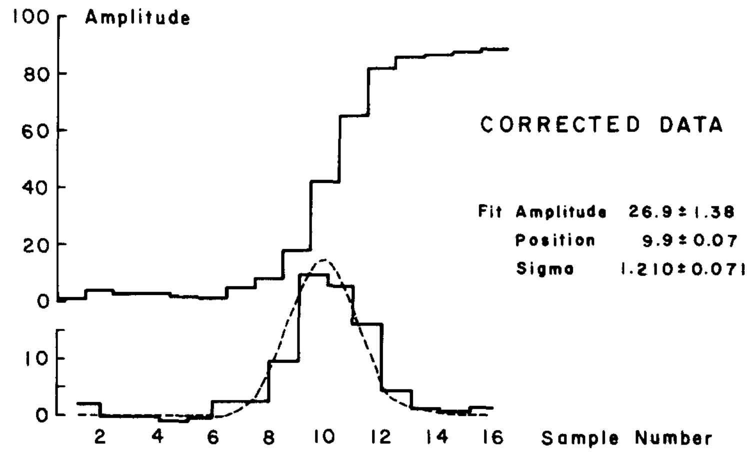

FIGURE 9. The same analysis as used in Fig. 5 applied to the average computed after pulses have been realigned to allow for the timing jitter. Parameters for the taller, narrower best fit curve are shown. Note the reduction in error estimates returned by the fit program.

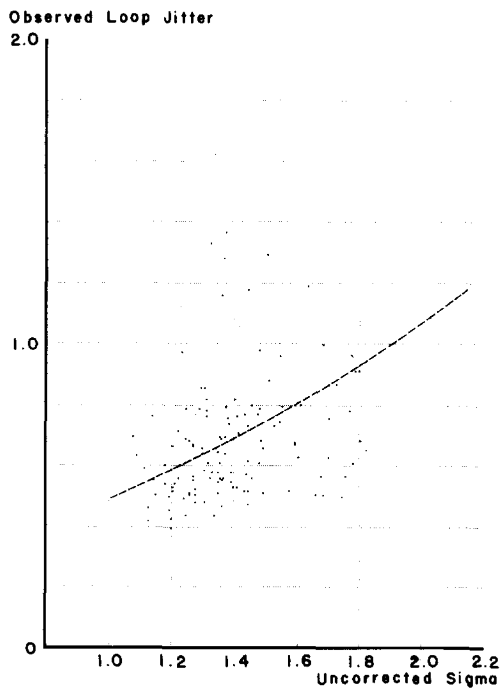

FIGURE 10. The relation between loop jitter standard deviation and the total standard deviation for uncorrected data as found in prelaunch tests (from a preliminary version of the "GEOS-C Altimeter data users handbook"). Points show individual values of loop jitter for each record of the pass discussed in the text. Both axes are in units of the sampling interval of 6.25 nsec.

nsec of the predicted line, but occasional large values occur which would lead to high indicated waveheights if uncorrected.

The tracker on the GEOS-3 satellite attempts to follow the variations in arrival time of pulses reflected from the sea surface, and to hold the leading edge of the return pulse stationary with respect to the 16 sample gates. The results discussed above show the extent to which the tracker fails to do this. These results do not show whether these timing variations are residuals remaining after real, rapid variations in range have been compensated or whether the observed jitter is introduced almost entirely by noise on the range steering signals in the tracking loop.

In fact it appears that the latter is true and that the timing errors can also be removed by assuming that the true range varies linearly during a 3.2 sec segment of data. Figure 11 illustrates this point. Here the timing variations found by the digital tracking algorithm described

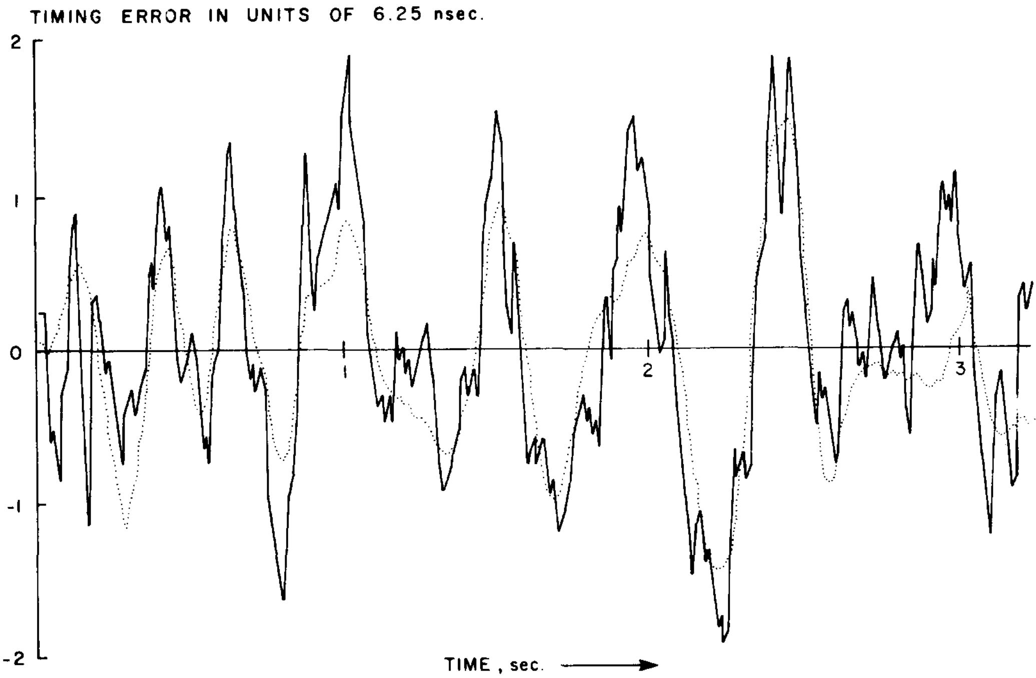

FIGURE 11. Timing errors for pulses in a frame of 320 pulses (3.2 sec of data). The dotted line is the output from the leading edge tracking algorithm described in the text. The solid line shows timing errors computed from the range servo error signals after subtraction of the best fitting linear trend.

above are plotted as a dashed line for one data segment. This shows that these variations have an rms value of 3.7 nsec for this segment and that the variations are concentrated towards high frequencies near the limit of the algorithm's response.

Values of the range servo error signal are also given in the 'high rate' data and represent quantified timing shifts that are applied to the set of 16 sampling gates before reception of the next pulse. If the cumulative effects of these timing changes are computed during a 3.2 sec data segment, then a strong linear trend is evident in the timing due to the changing range between the satellite and the sea surface. If this linear trend is removed by subtracting the best-fitting straight line from the timing changes, then the solid line in Fig. 11 results. This line shows larger timing variations, but there is evidently considerable agreement between the two curves, certainly for the lower frequency timing variations (up to about 4 Hz). It therefore appears that noise in the range servo signals is the predominant cause of the observed timing variations. The difference between the two curves still has an rms value of 2.8 nsec due mostly to the higher frequency components of this noise. Since these higher frequency timing changes have been applied to the gates, the solid curve should give a better representation of the timing errors that need to be removed from the data. On the other hand, any true range variations that are not linear over 3.2 sec will cause this representation to be in error. Sea surface slope changes sudden enough to cause such errors should be extremely rare, however.

A comparison of data corrected for timing variations calculated by the two different methods showed that the range servo error method resulted in slightly lower indicated waveheights having a slightly greater scatter. In short, the two methods seem about equally effective, and the difference between the results from the two methods is relatively small. Since the cumulative effect of the error signals is being computed, gaps in the data will disrupt the calculation. Such gaps occur in a few percent of the data segments but are not sufficiently frequent to be a severe problem or indeed to explain the larger scatter noted above.

In conclusion it appears that the range servo errors can be used to correct the timing variations before averaging the individual pulse shapes. This method has the advantage of requiring considerably less computation. If the linear approximation to the change in range within the 3.2-sec segments is found to be inaccurate for some cases, then shorter data segments can be used.

The results show that if 'high rate' data are available, a considerable reduction in scatter of the deduced waveheights can be achieved. As noted above, the simplest computation gives waveheights from each data segment which show a scatter of ± 1.6 meters about a 16 sec (5 data segments) running mean. Recalculation of the waveheights from the high rate data using the error function fit method, and the prelaunch values of loop jitter (curve in Fig. 10) reduces this scatter to ± 1.0 meters. The detailed correction for timing variations using the range servo error reduces this scatter to about ± 0.5 meters, while use of the range tracking algorithm gives a final scatter of ± 0.4 meters.

The revised $H_{\frac{1}{3}}$ values for the May 2,

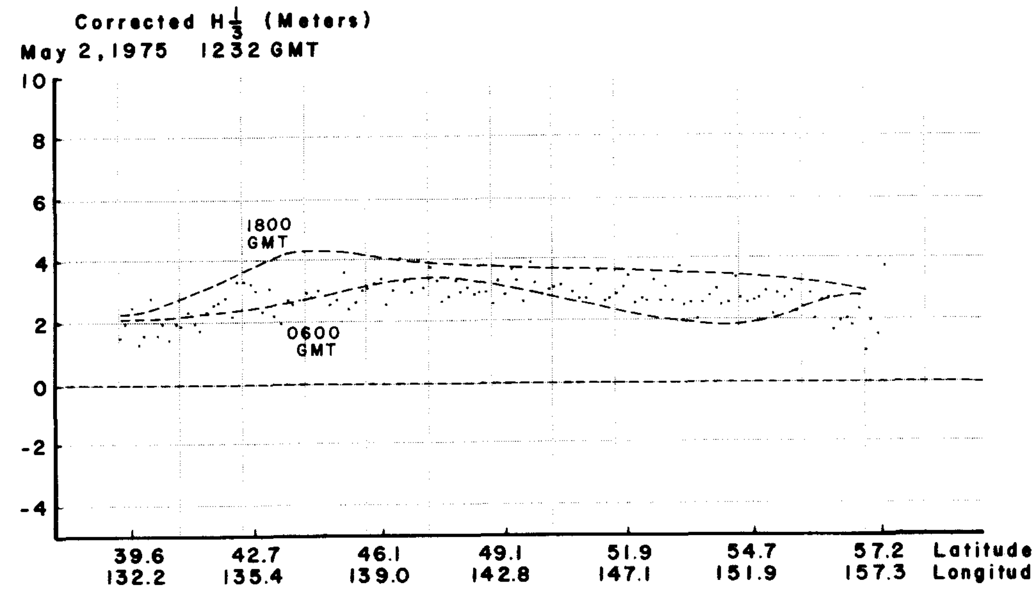

FIGURE 12. Values of $H_{\frac{1}{3}}$ computed from values of σ which have been corrected for the effects of loop jitter and bias errors as described in the text. The algorithm uses $\sigma_0 = 6.35$ nsec as the effective standard deviation of the transmitted pulse, and derives waveheights using a weighted error function fitting technique.

1975, satellite pass are plotted in Fig. 12 and can be compared with the values shown in Fig. 4. The reduction in scatter about a mean line (16 sec data average) is by a factor of roughly 3. The remaining scatter corresponds to ±0.5 m for each 3.2-sec data segment.

Comparison of GEOS-3 Data with Ground Truth

In all, 15 passes containing waveheight information have been received from NASA Wallops and analyzed. In four cases the satellite had transmitted data at the low rate so that only the analog averages of the pulse shapes were available. In six cases the satellite transmitted only 8 samples of each leading edge pulse shape, and an empirical correction for processing of this type of data was derived. The scatter value appropriate to these points appears to be about ±1 m. In the remaining five cases the full 16 samples were present and the corrections discussed above could be used.

Figure 13 shows the result of comparing satellite measurements with ground truth interpolated from charts such as those shown in Fig. 3. Apart from errors

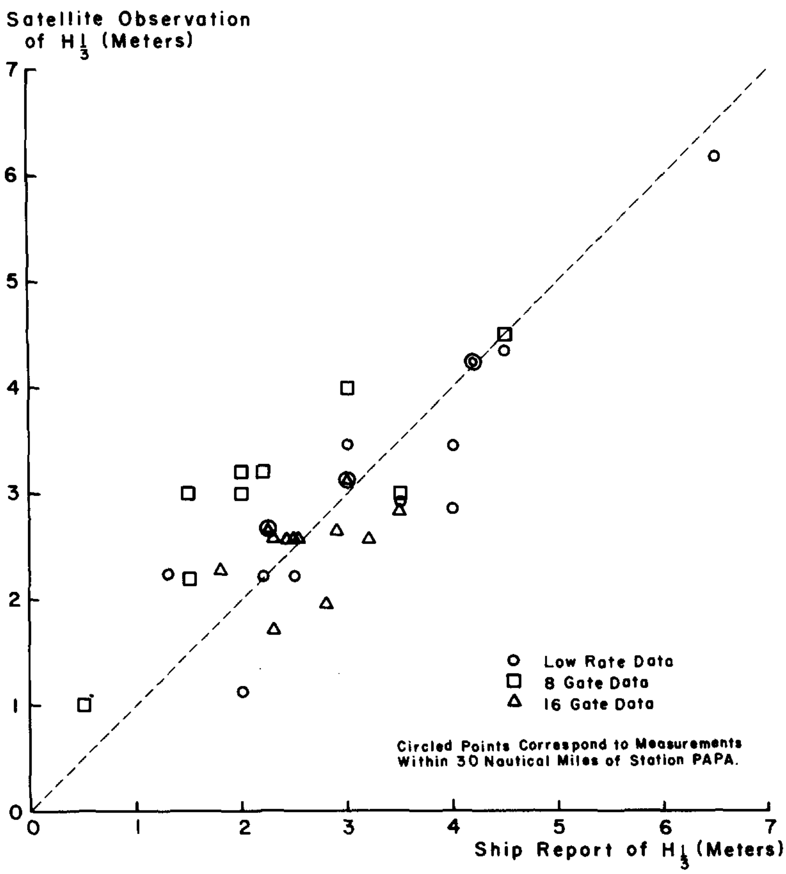

FIGURE 13. Comparison of GEOS-3 waveheight measurements with waveheights reported by ship observations and compiled on METOC charts. Circled points correspond to cases where the satellite has passed close to sation PAPA where waveheights are measured at 3 hour intervals with higher accuracy.

in both sources of data, the comparison is complicated by the different time and space coverage of ships and aircraft. The satellite data has been smoothed over roughly 20 sec so that the scatter discussed above should be correspondingly reduced. For the three ringed cases the satellite track passed with 55 km (30 nautical miles) of Ocean Weather Station PAPA where accurate measurements of waveheight are made at 3-hour intervals. From the observed short-term variability of PAPA data and the calibration tests that have been done there in the past, these measurements should be accurate to ± 0.2 meters. The waveheight scale of the satellite measurement contains the parameter σ_p which can in principle be determined from instrument calibration, but can most easily be deduced from comparisons with ground truth. From the data used to plot Fig. 13 the value $\sigma_p = 6.35 \pm 0.25$ nsec was deduced, as noted in previous sections of this paper.

It can be seen that agreement with station PAPA data is good (better than 0.5 m), but the other data show a larger scatter. In view of the probable inaccuracy of the ship data, and the time and distance differences between ship and satellite observations, the scatter in Fig. 13 could be almost entirely due to errors in the ground truth.

The study on the accuracy of visual wave observations reported by Cartwright (1962) in fact gives a plot of visual versus measured $H_{\frac{1}{3}}$ values which has a scatter very similar to that shown in Fig. 13. Cartwright's data were obtained from weatherships and the reports used here may be less accurate, but some confirmation and averaging was possible for the visual report values used in Fig. 13. The adjustment of the parameter σ_p made in this study affects lower calculated $H_{\frac{1}{3}}$ values much more strongly than higher ones. The fact that Fig. 13 indicates a best-fitting line which passes close to the origin is therefore a confirmation of this approach.

Several NOAA buoys capable of measuring and transmitting more accurate waveheight information have now been deployed in the study area, so that improved ground truth will be available for comparison with GEOS-3 data in the future.

Conclusions

The methods of analysis described above appear capable of giving a waveheight measurement with an accuracy of about ± 0.5 meters from a 3.2 sec average of GEOS-3 data. This time interval corresponds to 25 km along track. The result of the analysis of satellite data is to give a value for the best-fitting standard deviation (in meters) to the normal or gaussian sea surface height distribution due to waves. This standard deviation should therefore be simply related to the commonly reported significant waveheight $H_{\frac{1}{3}}$ independent of the wave spectrum actually present. Calibration and use of the data are therefore in priciple extremely simple, though the fact that the data give no information on wave spectrum or direction can also be seen as a disadvantage.

The satellite system is at present experimental and a rather small amount of data has so far been made available. This is at least partly because of the complex and precise calculations of satellite position needed for the altimeter range data to be used for geodetic purposes. Since waveheight calculations are independent of the indicated range, it should be possible to avoid these complications, and it is to be hoped that in future the wave data can be made available with considerably less delay and in much greater quantities.

In fact, the derivation of waveheights from GEOS-3 data is extremely direct in the sense of being uncomplicated by other environmental effects, and the high degree of spatial averaging achieved by the altimeter gives it an advantage over more conventional ground-based methods. With the present system of on-board pulse shape computation, the full 'high rate' data format is needed to calculate waveheights to the highest accuracy possible. There is no reason, in principle, why computations of the type described above should not be performed on board the spacecraft so that an operational waveheight measuring satellite could transmit real-time data on a simple narrow band link that could be received by many users.

Note added in proof. GEOS-3 wave data is now being rapidly calculated and distributed as suggested in the second paragraph of the conclusions above. Wave and wind data for selected satellite orbit segments are available with 6—12-hr delay on the commercial Infonet data system, and can be accessed by telephone terminal link according to date, orbit number, or geographical area. Wave data is computed by a simple algorithm similar to those described here for low rate data. Scatter is reduced by averaging over 11 data segments (about 25 sec). The surface wind information is deduced from the strength of the radar return. Further details are available from the GEOS-3 project office at NASA Wallops.

Acknowledgments

The author was accepted as a principle investigator for GEOS-3 by NASA and is grateful to them for the opportunity to work with this data. The METOC Office in Esquimalt, B.C., is gratefully acknowledged as the source of ship data and wave charts. The wave climate study group of Ocean and Aquatic Sciences in Ottawa provided the Station PAPA data.

This study would not have been possible without the work of Dawson Truax, who wrote and ran the series of programs for analysis of the altimeter data on an HP 2100 computer system.

References

Abramowitz, M., and Stegun, I. A. (1964), *Handbook of Mathematical Functions. National Bureau of Standards Applied Mathematics Series*, No. 55, U.S. Department of Commerce.

Barrick, D. E. (1972), Determination of mean surface position and sea state from the radar return of a short pulse satellite altimeter. Sea Surface Topography from Space, Vol. 1, Paper 16. NOAA Technical Report ERL 228-AOML 7.

Brown, G. S. (1977), The average impulse response of a rough surface and its applications, *IEEE Journal of Oceanic Engineering* (January 1977), Volume OE2, 67–74, and *IEEE Transactions on Antennas and Propagation* (January 1977), Volume AP 25, 67–74.

Cartwright, D. E. (1962), A comparison of instrumental and visually estimated waveheights and periods recorded on ocean weather ships. National Institute of Oceanography (UK), October 1962.

Godbey, T. W. (1976), Study of GEOS-3 altimeter performance characteristics for data management, calibration, and design criteria. Report prepared for NASA contract NAS6-2619. April 1976.

Greenwood, J. A., Nathan, A., Neuman, G., Pierson, W. J., Jackson, F. C., and Pease, T. E., (1969), Radar altimetry from a spacecraft and its potential applications to Geodesy. *Remote Sensing of Environment* 1, 59–70.

Greenwood, J. A., Nathan, A., Neuman, G., Pierson, W. J., Jackson, F. C., and Pease, T. E., (1969), Oceanographic applications of radar altimetry from a spacecraft. *Remote Sensing of Environment* 1, 71–80.

Hofmeister, E. L. (1969), Analysis and measurement of the performance of a signal tracking loop for a satellite radar altimeter. Technical Information Series R 76EML7, General Electric Aerospace Electronic Systems Department, April 1976.

Hofmeister, E. L., Keeney, B. N., Godbey, T. W., and Berg, R. J. (1976), Data users handbook and design error analysis, GEOS-C radar altimeter, Vol. I, May 1976, Report prepared for NASA contract NAS6-2619.

Longuet-Higgins, M. S. (1952), On the statistical distribution of the heights of sea waves. *Journal of Marine Research* 11, 245–266.

Miller, L. S., and Hayne, G. S. (1972), Characteristics of ocean-reflected short radar pulses with application to altimetry and surface roughness determination. Sea Surface Topography from Space, Vol. I, paper 12. NOAA Technical Report ERL 228-AOML 7.

Shapiro, A., Uliana, E. A., and Yaplee, B. S. (1972), Radar pulse shape versus ocean waveheight. Sea Surface Topography from Space, Vol. I, paper 11. NOAA Technical Report ERL 228-AOML 7.

Wilson, J. R. and Baird, W. F. (1972), A discussion of some measured wave data. Proceedings of the 13th Coastal Engineering Conference, Vancouver, B.C. Canada, July 1972, page 113.

Received 7 June 1977; revised 30 January 1978